

# Using a cylindrical vortex model to assess the induction zone infront of aligned and yawed rotors

**Branlard, Emmanuel Simon Pierre; Meyer Forsting, Alexander**

*Published in:*
Proceedings of EWEA Offshore 2015 Conference

*Publication date:*
2015

*Document Version*
Publisher's PDF, also known as Version of record

# Using a cylindrical vortex model to assess the induction zone in front of aligned and yawed rotors

Emmanuel Branlard, Alexander R. Meyer Forsting

*DTU, Wind Energy, Denmark*

February 19, 2016

**Abstract**

Analytical formulae for the velocity field induced by a cylindrical vortex wake model are applied to assess the induction zone in front of aligned and yawed rotors. The results are compared to actuator disk (AD) simulations for different operating conditions, including finite tip-speed ratios. The mean relative error is estimated in the induction zone and found to be below 0.4% for the aligned flows tested and below 1.3% for the yawed test cases. The computational time required by the analytical model is in the order of thousands of times less than the one required by the actuator disk simulation.

## 1 Introduction

The interest in the flow behaviour inside the induction zone, which develops in front of a wind turbine rotor, has re-emerge over the last decade. Simley compared lidar measurements with Computational Fluid Dynamics (CFD) simulations [14]. A better knowledge of the induction zone can improve control strategies. In recent work, the possibility that the wind turbine influences the turbulence characteristics in the induction zone has been investigated [4]. Based on analyses of the turbulence spectrum, it appeared that the approximation that the turbulence characteristics remained unaffected by the turbine was fair upstream of the turbine. The standards recommend a distance of 2.5 diameters to locate a meteorological mast and measure the representative free-stream velocity [10]. The possible effect of the turbine induction at this location can be quantified as mentioned in previous work by the authors [2].

The current paper uses the cylindrical rotor model of Joukowski [11] to determine the velocity field developing in the induction zone. The model was recently applied by the authors to aligned [2] and yawed conditions [3], where closed form expressions or semi-empirical expressions can be obtained for the entire flow field, respectively. Superposing such models can add further detail to the flow [5].

The paper briefly presents the analytical models needed to assess the velocity field upstream of the rotor. Results are then compared to CFD - actuator disk (AD) simulations in aligned and yawed conditions.

## 2 Model for the velocity field in the induction zone

### 2.1 Presentation of the model

The vortex cylinder (VC) model represents an actuator disk and its wake by assuming a prescribed support of vorticity in line with the cylindrical model of Joukowski [11]. The rotor and

its wake are assumed to be contained within a cylinder. The cylinder axis forms an angle $\chi$ with respect to the normal of rotor disk in case of a yawed inflow. This angle is referred to as the "skew" angle and is usually higher than the yaw angle [7]. The term "aligned flow" will be used when $\chi = 0$. When the circulation is constant along the span of the rotor disk, the model is said to be an "elementary" model. The model for a radial variation of circulation is detailed in subsection 2.4. The azimuthal variation of circulation is not accounted for in the current study. That the assumption of constant circulation produces satisfying results has been proven by many Blade Element Momentum (BEM) codes relying on this simplification for their yaw models [9, 6]. The elementary model consists of the following components of vorticity: a root vortex, a semi-infinite vortex cylinder with tangential $\gamma_t$ and longitudinal vorticity $\gamma_l$, and a bound vortex disk with radial vorticity $\gamma_b$. The elementary cylindrical vortex model considered and the coordinate system used are shown in Figure 1. The generation of this vortex system

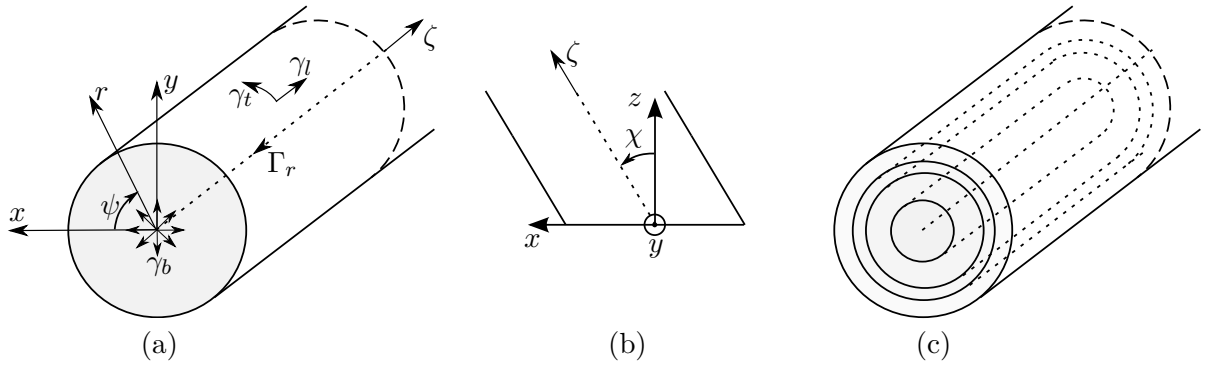


Figure 1: Vortex model and coordinate system. (a) Elementary system. (b) Positive definition of the skew angle $\chi$. (c) Concentric superposition of elementary systems.

behind an actuator disk is discussed by van Kuik [16]. For simplicity, the current models neglects wake expansion. This assumption is discussed in detail in [5]. The notation $u_{\bullet,\diamond}$ will refer to the $\bullet$-component of the velocity induced by the vortex element $\diamond$, where $\bullet \in \{r, \psi, z\}$ and $\diamond \in \{r, t, l, b\}$. The velocity field induced by the full vortex system is: $u_r = u_{r,t} + [u_{r,l} + u_{r,r}]$, $u_z = u_{z,t} + [u_{z,l} + u_{z,r}]$, $u_\psi = u_{\psi,l} + u_{\psi,r} + u_{\psi,b} + [u_{\psi,t}]$ where the terms in square brackets are zero in the aligned case. The following notations are further introduced: $\Gamma_{\text{tot}}$ is the total circulation of the rotor, $R$ is the rotor radius, and $h$ is the pitch of the helical wake formed by the combination of the two tip-vorticity components $\gamma_t$ and $\gamma_l$.

## 2.2 Formulae in the aligned case for the elementary model

The different strengths of the root vortex, the bound vorticity, the tangential and longitudinal vorticity are respectively [2]:

$$\boldsymbol{\Gamma}_r = -\Gamma_{\text{tot}}\, \boldsymbol{e}_z, \qquad \boldsymbol{\gamma}_b(r) = \frac{\Gamma_{\text{tot}}}{2\pi r}\, \boldsymbol{e}_r, \qquad \boldsymbol{\gamma}_t = -\frac{\Gamma_{\text{tot}}}{h}\, \boldsymbol{e}_\psi, \qquad \boldsymbol{\gamma}_l = \frac{\Gamma_{\text{tot}}}{2\pi R}\, \boldsymbol{e}_z, \tag{1}$$

The expressions of the different components were obtained by direct integration of the Biot-Savart law as [2]:

$$
\begin{aligned}
u_r(r,z) &= -\frac{\gamma_t}{2\pi}\sqrt{\frac{R}{r}}\left[\frac{2-\mathrm{k}^2(r,z)}{\mathrm{k}(r,z)}K\left(\mathrm{k}^2(r,z)\right)-\frac{2}{\mathrm{k}(r,z)}E\left(\mathrm{k}^2(r,z)\right)\right]\\
u_z(r,z) &= \frac{\gamma_t}{2}\left[\frac{R-r+|R-r|}{2|R-r|}+\frac{z\mathrm{k}(r,z)}{2\pi\sqrt{rR}}\left(K\left(\mathrm{k}^2(r,z)\right)+\frac{R-r}{R+r}\Pi\left(\mathrm{k}^2(r,0),\mathrm{k}^2(r,z)\right)\right)\right] \qquad (2)\\
u_\psi(r,z) &= \begin{cases} -\Gamma_{\mathrm{tot}}/4\pi r, & r<R \text{ and } z=0 \quad \text{, or,} \quad r=R \text{ and } z>0\\ -\Gamma_{\mathrm{tot}}/2\pi r, & r<R \text{ and } z>0\\ 0, & \text{otherwise}\end{cases}
\end{aligned}
$$

where $E$, $K$ and $\Pi$ are the complete elliptic integrals of the first, second and third kind respectively, where the elliptic parameter k is given by

$$
\mathrm{k}^2(r,z)=\frac{4rR}{(R+r)^2+z^2}, \qquad n_1=\frac{2r}{r+\sqrt{r^2+z^2}}, \qquad n_2=\frac{2r}{r-\sqrt{r^2+z^2}}. \qquad (3)
$$

and where $n_1$ and $n_2$ are used below. The different components forming the tangential velocity are:

$$
u_{\psi,l}(r,z)=\frac{\gamma_l}{2}\frac{R}{r}\left[\frac{r-R+|R-r|}{2|R-r|}+\frac{z\mathrm{k}(r,z)}{2\pi\sqrt{rR}}\left(K\left(\mathrm{k}^2(r,z)\right)-\frac{R-r}{R+r}\Pi\left(\mathrm{k}^2(r,0),\mathrm{k}^2(r,z)\right)\right)\right] \qquad (4)
$$

$$
u_{\psi,r}(r,z)=-\frac{\Gamma_{\mathrm{tot}}}{4\pi r}\left[1+\frac{z}{\sqrt{r^2+z^2}}\right] \qquad (5)
$$

$$
u_{\psi,b}(r,z)=\frac{\Gamma_{\mathrm{tot}}}{4\pi}\left\{\frac{1}{r}\left[\frac{z}{\sqrt{r^2+z^2}}-\frac{|z|}{z}\right]-\frac{1}{\pi z}\sqrt{\frac{r}{R}}\frac{z^2}{r^2}\,\mathrm{k}\left[K(\mathrm{k}^2)+T_1\,\Pi(n_1,\mathrm{k}^2)-T_2\,\Pi(n_2,\mathrm{k}^2)\right]\right\} \qquad (6)
$$

$$
T_1=\frac{\left(\sqrt{r^2+z^2}-r\right)(r+R)-z^2}{2z^2}, \qquad T_2=\frac{\left(\sqrt{r^2+z^2}+r\right)\left(\sqrt{r^2+z^2}+R\right)}{2z^2}, \qquad (7)
$$

### 2.3 Formulae in the yawed case for the elementary model

The different strengths of the root vortex, the bound vorticity, the tangential and longitudinal vorticity are respectively [3]:

$$
\boldsymbol{\Gamma}_r=-\Gamma_{\mathrm{tot}}\,\boldsymbol{e}_z, \qquad \boldsymbol{\gamma}_b(r)=\frac{\Gamma_{\mathrm{tot}}}{2\pi r}\,\boldsymbol{e}_r, \qquad \boldsymbol{\gamma}_t=-\frac{\Gamma_{\mathrm{tot}}}{h/\cos\chi}\,\boldsymbol{e}_\psi, \qquad \boldsymbol{\gamma}_l=\frac{\Gamma_{\mathrm{tot}}}{2\pi R}\,\boldsymbol{e}_\zeta \qquad (8)
$$

**Velocities induced by the tangential vorticity** The velocity induced by the tangential vorticity was first studied by Coleman [9], then extended by Castles and Durham [8] and recently generalized by Branlard and Gaunaa [3]. The velocity is obtained using an analytical integration over $z$ and a numerical integration over $\psi$ to give:

$$
\begin{aligned}
u_{\bullet,t}(r,\psi,z) &= \frac{\gamma_t}{4\pi}\int_0^{2\pi}\frac{2\left(a'_\bullet\sqrt{c}+b'_\bullet\sqrt{a}\right)}{\sqrt{a}\left(2\sqrt{ac}+b\right)}\,d\theta' \qquad (9)\\
\{a'_z,\ b'_z\} &= R\,\{R-r\cos(\theta'-\psi),\ m\cos\theta'\}\\
\{a'_r,\ b'_r\} &= R\,\{z\cos(\theta'-\psi),\ -\cos(\theta'-\psi)\}\\
\{a'_\psi,\ b'_\psi\} &= R\,\{z\sin(\theta'-\psi),\ -\sin(\theta'-\psi)\}\\
\{a,\ b,\ c\} &= \left\{R^2+r^2+z^2-2rR\cos(\theta'-\psi),\ 2mR\cos\theta'-2mr\cos\psi-2z,\ 1+m^2\right\}
\end{aligned}
$$

where the symbol $\bullet$ stands indifferently for $r, \psi, z$ and where $m = \tan\chi$. In the rotor plane, and for $\psi = 0$ the integration over the azimuthal variable can be carried on analytically. An analytical formula was given by Coleman et al. [9] for the velocity inside the rotor and by the first author for the velocity outside of the rotor [1]:

$$u_{z,t}(r > R, \psi = 0, z = 0) = \frac{\gamma_t}{2}(1 + K_i + K_o) \tag{10}$$

$$K_i(r, \chi) = 2F_t(r, \chi)\tan\frac{\chi}{2}$$

$$K_o(r, \chi) = -\frac{r\sqrt{1+m^2}}{2m^2\left(r^2 - R^2\right)}\left(\frac{r\left(\sqrt{C-B}+\sqrt{B+C}\right)}{\sqrt{r^2+m^2R^2}} + \frac{\sqrt{C-B}-\sqrt{B+C}}{\sqrt{1+m^2}}\right)$$

with $F_t(r, \chi) = \frac{K_i(r,\chi)}{2\tan\frac{\chi}{2}} \approx r/2R$ and

$$B = 2r\sqrt{(1+m^2)(r^2+m^2R^2)}, \quad C = (2+m^2)r^2 + m^2R^2$$

The exact expression for $K_i$ is given in the article of Coleman et al. Equation 10 can be used to verify the numerical integration performed in Equation 9 for the axial induction. The azimuthal variation of the axial velocity is modelled based on the value at the fore-aft diameter as:

$$u_{z,t}(r < R, \psi, z = 0) \approx \frac{\gamma_t}{2}\left[1 + K_i(r)\cos(\psi)\right] \tag{11}$$

$$u_{z,t}(r > R, \psi, z = 0) \approx \frac{\gamma_t}{2}\left[(1 + K_o(r))\cos(2\psi) + K_i(r)\cos\psi\right] \tag{12}$$

The model values are exact for $\psi = 0°$ and $\psi = 90°$.

**Other components** In the current paper, yawed simulations will be performed for an infinite tip-speed ratios so that only the tangential component of vorticity contributes to the flow. The induced velocities originating from other components were already derived in previous work [3] and will be tested against actuator disk simulations in the future.

### 2.4 Extension to a varying circulation along the span

The velocity field of a rotor with varying circulation along its span is obtained using a superposition of the velocity fields given in the previous sections. The superposition of cylinders is illustrated in Figure 1c. The determination of the cylinder strengths from the thrust distribution is done according to previous work published on this topic [5].

## 3 Results

Actuator disk simulations were carried out using the in-house 3D flow solver EllipSys3D, developed by Michelsen and Sørensen [13, 15]. Results from these simulations are used as a reference to assess the quality of the velocity field obtained from the analytical model.

### 3.1 Aligned case, without swirl

The results presented in this paragraph were performed for a constant thrust coefficient prescribed along the span. Further, the actuator disk is not rotating. This which is similar to $\lambda = \infty$ for which only the tangential vorticity component is present. In the absence of swirl, a constant thrust coefficient implies a constant circulation distribution. As a result of this,

one vortex cylinder is enough to model the flow. For ease of comparison, the value of $\gamma_t$ was obtained by extracting the induced velocity at the middle of the rotor plane from the Actuator disk simulation. Indeed according to the vortex cylinder model, $u(r = 0, z = 0) = \gamma_t/2$. The axial and radial velocities along the rotor's axis $x = 0$ and along the rotor radius $z = 0$ are shown in Figure 2 for two different $C_T$ values. The coefficients of determination $R^2$ between the

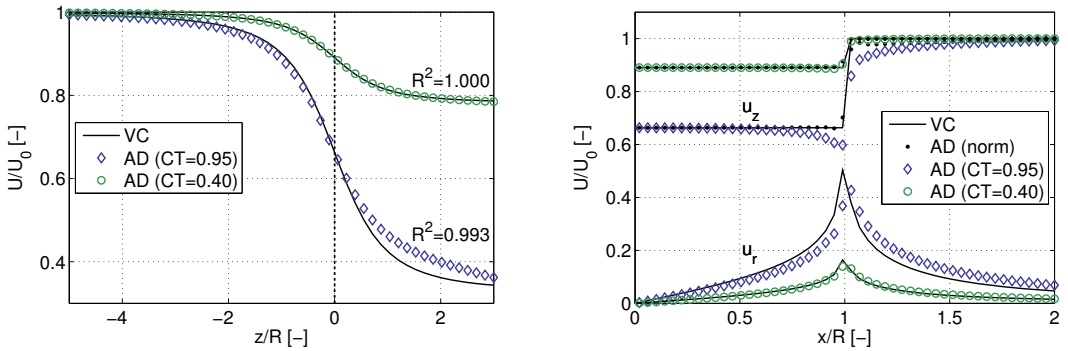


(a) (b)

Figure 2: Axial and radial velocities along the rotor's axis (left) and along the rotor radius (right) for two different $C_T$ values.

curves are also shown in the figure. It is reminded that along the $z$ axis, Equation 2 reduces to (see e.g. [2]):

$$u_z(r = 0, z) = \frac{\gamma_t}{2}\left[1 + \frac{z}{\sqrt{R^2 + z^2}}\right] \tag{13}$$

The figure shows that the AD and VC results are in strong agreement for low values of the thrust coefficient, where the omission of the wake expansion is indeed justifiable. Discrepancies arises at higher thrust coefficients. In particular, the axial induction obtained from the AD simulations are not constant over the rotor span as opposed to what is predicted by the VC theory. On the other hand, the velocity norm on the rotor plane is close to constant. These observations were also presented by van Kuik and Lignarolo [17].

The full velocity fields for the challenging case of $C_T = 0.95$ are compared for the numerical and analytical model in Figure 3.

### 3.2 Aligned case with swirl

Simulations including swirl cannot be carried out with a constant thrust coefficient along the span, as it would result in infinite tangential velocities at the root [5]. In line with the work of Madsen et al. [12], the thrust coefficient is prescribed to a constant $C_{T_0}$ along most of the span and drops linearly to zero from the radial position $r/R = 0.11$ towards the root. For convenience the subscript 0 is dropped in the rest of the document. For the VC model, the circulation is determined by solving the following equation for $k$ at each radial position [5]:

$$k(r)\left(1 + \frac{k(r)}{4\lambda_r^2}\right) - C_{t,in}(r) = 0 \tag{14}$$

The vortex cylinder strengths are then determined using the pitch angle of the helix [5]. An example of the axial velocity contours obtained for $C_T = 0.4$ is shown in Figure 4. The two models strongly agree in the induction zone, and predict the high velocity core towards the root

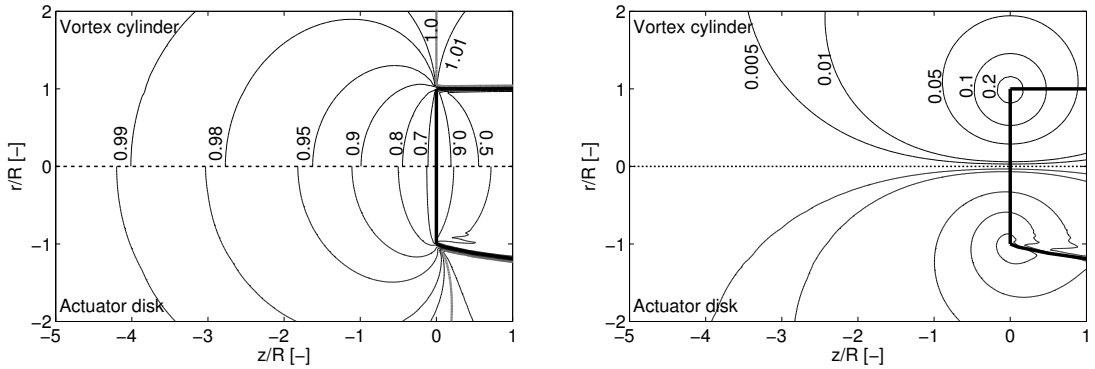


(a) (b)

Figure 3: Contours of axial (left) and radial (right) velocities normalized by the free stream for a thrust coefficient $C_T = 0.95$ and for both the actuator disk and vortex cylinder model. The lack of wake expansion in the vortex cylinder model is the main source of discrepancy between the two models.

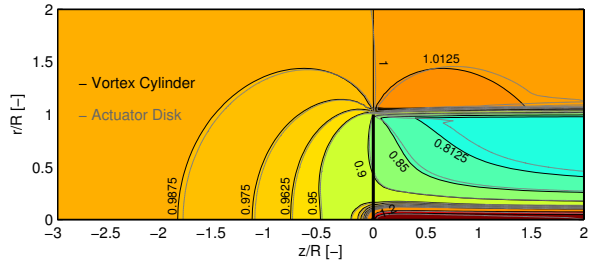


Figure 4: Axial velocity contours for an aligned flow with swirl $C_T = 0.4$, $\lambda = 2$. The contours for the vortex cylinder are plotted in black while the ones from the actuator disk are plotted in gray.

of the blade. Progressively downstream of the rotor the discrepancies keep increasing, due to the wake expansion present in the CFD simulation.

A parametric study is performed to quantify the error of the axial induction predicted by the vortex cylinder model for different operating conditions $(C_T, \lambda)$. Results are reported in Table 1. The induction zone was defined as the rectangular area delimited by $r, z \in [-0.9R, 0.9R] \times [-3R, 0R]$. The vortex cylinder singularity towards $R = 1$ was avoided in this manner. A regularized vortex cylinder formulation can also be used to avoid this singularity [1]. The error is highest, as expected, for high thrust coefficients, due to the lack of wake expansion in the vortex model. Overall the induction zone is predicted with an average accuracy of 0.4%.

Table 1: Relative error in axial velocity in the induction zone for different operating conditions.

| | $C_T = 0.4$ | | | | $C_T = 0.95$ | | | |
|---|---|---|---|---|---|---|---|---|
| | $\lambda = 2$ | $\lambda = 6$ | $\lambda = 10$ | $\lambda = \infty$ | $\lambda = 2$ | $\lambda = 6$ | $\lambda = 10$ | $\lambda = \infty$ |
| Mean | 0.1% | 0.1% | 0.1% | 0.0% | 0.1% | 0.2% | 0.3% | 0.4% |
| Max | 0.2% | 0.2% | 0.2% | 0.2% | 1.8% | 2.5% | 2.7% | 3.3% |

### 3.3 Yawed case

Simulations of a yawed rotor without swirl are presented in this paragraph. The actuator disk simulations were run for a yaw angle of $\theta_{\text{yaw}} = 30°$. The loading on the actuator disk was prescribed using a constant thrust coefficient. The vortex cylinder model assumed a constant circulation along the span. The skew angle required by the vortex cylinder model is determined using the following empirical relation [7, p. 105]:

$$\chi = \theta_{\text{yaw}} \left[1 + 0.6\,\overline{a}\right] = \theta_{\text{yaw}} \left[1 + 0.3\left(1 - \sqrt{1 - C_T}\right)\right] \tag{15}$$

where the mean induction was estimated as $\overline{a} = \frac{1}{2}\left(1 - \sqrt{1 - C_T}\right)$. An azimuthal variation of the loading and circulation is expected in a realistic simulation of an actuator disk in yawed inflow. The assumption made here was discussed in subsection 2.1. Figure 5 presents the same axial velocity profiles as Figure 2 but for $\theta_{\text{yaw}} = 30°$. In the left of this figure, the induction is

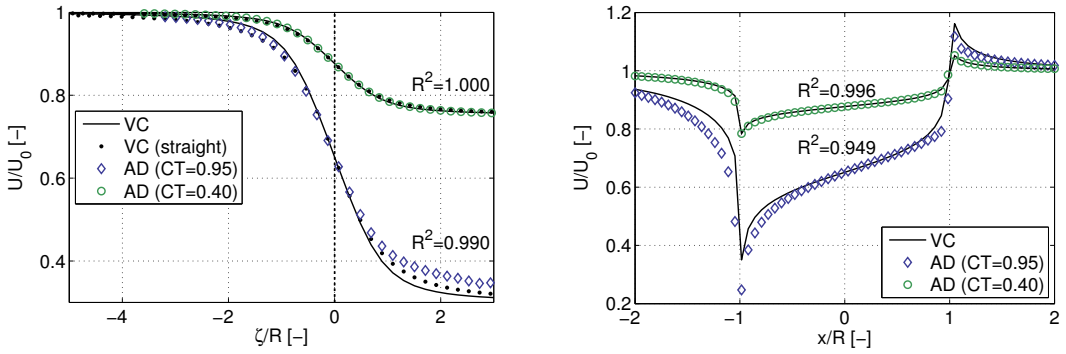


(a) (b)

Figure 5: Axial velocity along the rotor's axis (left) and along the rotor radius (right) for two different values of $C_T$. The curve labelled 'VC (straight)' corresponds to the evaluation of Equation 13 with $z = \zeta$.

plotted along the wake axis $\zeta$. The curve labelled 'VC (straight)' corresponds to the evaluation of Equation 13 with $z = \zeta$. It is seen that along the wake axis this formula is still of reasonable accuracy even for a yaw angle as large as 30°. The agreement between the AD and VC for the yawed case is slightly less than in the non-yawed case. The induction agrees to a high degree for the thrust coefficient $C_T = 0.4$. The same conclusions are drawn for the axial induction within the rotor plane as plotted in the right of the figure.

Axial velocity contours for two values of the thrust coefficients are shown in Figure 6. The agreements is fair for the low thrust coefficient case, whereas the marked differences in wake expansion observed in the right of the figure for $C_T = 0.95$ lead to visible differences in the velocity contours. These differences are further quantified. The absolute value of the relative error, scaled with the free-stream velocity, between the actuator disk and vortex cylinder models is shown in Figure 7. The induction zone as defined earlier is marked on the figure using a dashed box. The mean and maximum relative error within the induction zone is computed and shown on the figure. The mean relative error in the challenging case of high thrust coefficient $C_T = 0.95$ is 1.3%. The differences are the strongest close to the rotor where the effect of expansion has more impact.

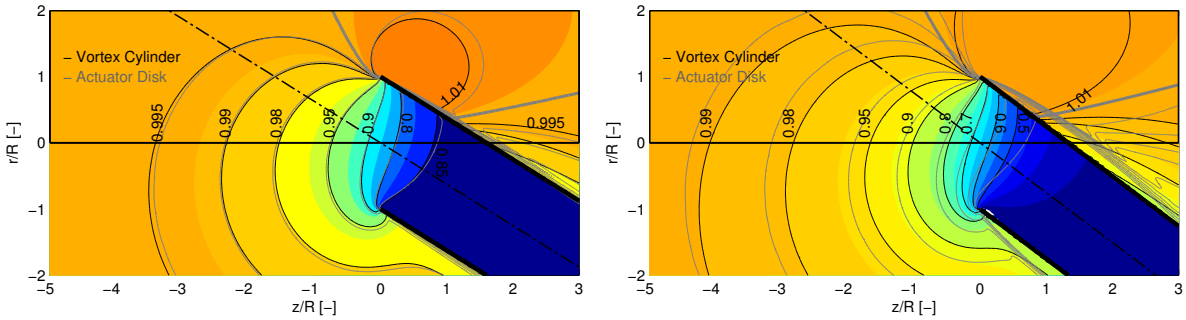


Figure 6: Axial velocity contours obtained with the two models for two values of the thrust coefficients. (left:) $C_T = 0.4$, (right:) $C_T = 0.95$

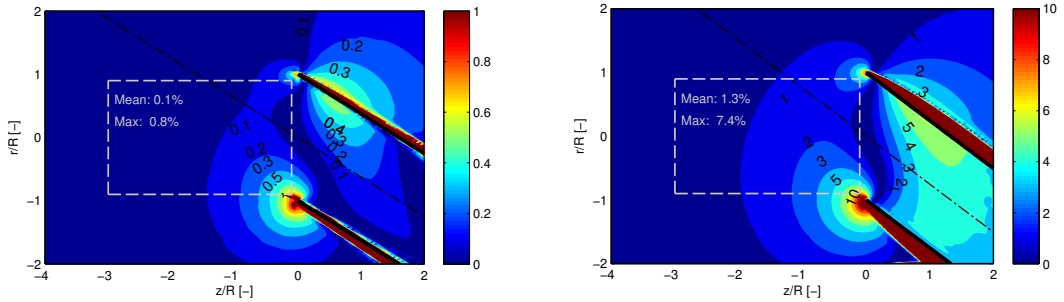


(a) (b)

Figure 7: Absolute value of the relative error in axial induction obtained by the vortex cylinder model compared to the actuator disk simulation for two thrust coefficients. (left:) $C_T = 0.4$, (right:) $C_T = 0.95$. The area marked with a dashed box refers to the "induction zone" for which the mean and maximum error are computed.

### 3.4 Computational time

The computational time on one CPU of the full velocity field for the vortex cylinder model takes approximately $1s$ using a non-compiled scripting language. The actuator disk simulations were run on 8 CPUs using a compiled language. If these simulations were run on one CPU the simulation times would be 2400s and 6000s for the simulations with swirl and without swirl respectively. In light of this difference of computational time the accuracy obtained by the vortex cylinder model are remarkable.

## 4 Conclusions

The velocity field from the analytical formulae of the cylindrical vortex wake model agreed to a high degree with the ones obtained from actuator disk simulations. For the aligned flow, a mean relative error of 0.4% was obtained in the induction zone. In the yawed condition tested, a mean relative error of 1.3% was obtained in the induction zone for the challenging case of $C_T = 0.95$ and $\chi = 30°$. The computational time required by the analytical model is in the order of thousands of times less than the one required by the actuator disk simulation. The model can be used for rapid estimates of the induction zone with a remarkable accuracy.

## References


[1] Branlard, E. *Analysis of wind turbine aerodynamics and aeroelasticity using vortex-based methods*. PhD thesis, Technical University of Denmark (DTU), Wind Energy Department, 2015.

[2] Branlard, E., and Gaunaa, M. Cylindrical vortex wake model: right cylinder. *Wind Energy 18*, 11 (2015), 1973–1987.

[3] Branlard, E., and Gaunaa, M. Cylindrical vortex wake model: skewed cylinder, application to yawed or tilted rotors. *Wind Energy* (2015), 1–14. we.1838.

[4] Branlard, E., and Gaunaa, M. Impact of a wind turbine on turbulence: un-freezing the turbulence by means of a simple vortex particle approach, 2015. (Submitted to the Journal of Wind Engineering and Industrial Aerodynamics, February 2015).

[5] Branlard, E., and Gaunaa, M. Superposition of vortex cylinders for steady and unsteady simulation of rotors of finite tip-speed ratio. *Wind Energy* (2015), 1–17. we.1899.

[6] Branlard, E., Gaunaa, M., and Machefaux, E. Investigation of a new model accounting for rotors of finite tip-speed ratio in yaw or tilt. *Journal of Physics: Conference Series (Online) 524*, 1 (2014), 1–11.

[7] Burton, T., Sharpe, D., Jenkins, N., and Bossanyi, E. *Wind Energy Handbook*, first ed. J. Wiley & Sons, New-York, N.Y., 2002.

[8] Castles, W., and De Leeuw, J. H. The normal component of the induced velocity in the vicinity of a lifting rotor and some examples of its application. Tech. rep., NACA Report No. 1184, Giorgia Institure of Technology, Atlanta, 1954.

[9] Coleman, R. P., Feingold, A. M., and Stempin, C. W. Evaluation of the induced-velocity field of an idealized helicopter rotor. *NACA ARR No. L5E10* (1945), 1–28.

[10] International Standard IEC. *IEC 61400-12 Power performance measurements of electricity producing wind turbines*. International Electrotechnical Commission, Geneva, 2005.

[11] Joukowski, N. E. Vortex theory of screw propeller, I. *Trudy Otdeleniya Fizicheskikh Nauk Obshchestva Lubitelei Estestvoznaniya 16*, 1 (1912), 1–31. (in Russian). French translation in: Théorie tourbillonnaire de l'hélice propulsive. Gauthier-Villars: Paris, 1929; 1: 1-47.

[12] Madsen, H., Bak, C., Døssing, M., Mikkelsen, R., and Øye, S. Validation and modification of the blade element momentum theory based on comparisons with actuator disc simulations. *Wind Energy 13* (2010), p373–389.

[13] Michelsen, J. A. *Block Structured Multigrid Solution of 2D and 3D elliptic PDE's*. AFM 94-05 - Department of Fluid Mechanics, Technical University of Denmark, 1994.

[14] Simley, E., Pao, L. Y., Gebraad, P., and Churchfield, M. Investigation of the impact of the upstream induction zone on lidar measurement accuracy for wind turbine control applications using large-eddy simulation. *Journal of Physics: Conference Series 524*, 1 (2014), 012003.

[15] Sørensen, N. N. *General Purpose Flow Solver Applied to Flow over Hills*. PhD thesis, Risø National Laboratory., 1995.

[16] van Kuik, G. A. M. On the generation of vorticity by force fields in rotor- and actuator flows. *Renewable Energy 70* (2014), 124–128.

[17] van Kuik, G. A. M., and Lignarolo, L. E. M. Potential flow solutions for energy extracting actuator disc flows. *Wind Energy Online* (2015), 1–16.